Available online at www.sciencedirect.com

SCIENCE DIRECT®

Journal of Power Sources 156 (2006) 369–374

JOURNAL OF POWER SOURCES

www.elsevier.com/locate/jpowsour

Predicting the transient response of a serpentine flow-field PEMFC II: Normal to minimal fuel and AIR

S. Shimpalee[a], W.-K. Lee[a], J.W. Van Zee[a,*], H. Naseri-Neshat[b]

[a] Department of Chemical Engineering, University of South Carolina, Columbia, SC 29208, USA
[b] Department of Mechanical Engineering Technology, South Carolina State University, Orangeburg, SC 29117, USA

Received 26 April 2005; accepted 20 May 2005
Available online 22 July 2005

Abstract

The three-dimensional (3D) transient model presented in part I is used to study the overshoot and undershoot behavior observed in a PEMFC during operation with fixed normal stoichiometic flow rates of hydrogen and air for a 1.0 V s^{-1} change in the load. In contrast to the behavior with excess flow shown in part I, the predictions show second-order responses for both decreases and increases in the load. That is, there is current overshoot when the load cell is decreased from 0.7 V to 0.5 V and there is current undershoot when the cell voltage is increased from 0.5 V to 0.7 V. The simulation of a 10 cm^2 reactive area with a serpentine flow path is used to explain this behavior in terms of the reacting gas concentrations, the flow through the gas diffusion media, the movement of water through the MEA by electro-osmotic and back diffusion forces, and the variation in the distributions of current density. The operating conditions correspond to 101 kPa, 70 °C cell temperature, anode and cathode dew-points and stoichiometries of 65 °C and 57 °C and 1.45 and 2.42 at an initial operating voltage of 0.7 V and current density of 0.33 A cm^{-2}. The fixed flow rates correspond to stoichiometries of 1.05 and 1.73 at 0.5 V for the 0.46 A cm^{-2} predicted current density. The predictions illustrate regions where the MEA may alternate between wet and dry conditions and this may be useful to explain stability and durability of the MEA during transient operation.

Keywords: PEM; Fuel cells; Membrane electrode assembly; Electric vehicle; Dynamic response; Overshoot

1. Introduction

Transient load changes during operation of PEMFCs with fixed gas flow rates may expose the MEA to various degrees of stoichiometry for either stationary or automotive applications. This transient operation may be a result of a sudden demand as an appliance starts or as a vehicle is accelerated or decelerated. Further these transients may be of sufficient magnitude and speed that gas flow rates cannot be adjusted by feedback control or that the capacitors in the system cannot accommodate the demand. Thus, the fuel cell by default or design may need to act as a capacitor during the power demand surge. The use of a mathematical model and a time-dependent three-dimensional (3D) equation solver is presented here to illustrate situations where the current does not change in a typical first-order manner between steady states. In fact we have observed experimentally [1–3] and through our predictions that the current can exhibit pseudo second-order behavior with overshoots and undershoots of the current.

In part I of this series [4], we presented a time-dependent 3D model and the corresponding simulation results that showed the effect of anode stoichiometry and rate of voltage change on the transient response of a 10 cm^2 PEMFC with a serpentine flow field. That paper considered the response when the flow of gas was large, exceeding a stoichiometry of 2.6/4.4[1] for 0.7 V and 1.2/2.0 for 0.5 V (i.e.,

* Corresponding author. Tel.: +1 803 777 2285; fax: +1 803 777 8142.
E-mail address: vanzee@engr.sc.edu (J.W. Van Zee).

[1] Our notation for specifying operating conditions is to list the anode conditions first followed by the cathode. Thus, the stoic was 2.6 for the anode and 4.4 for the cathode. This relates to 160% excess hydrogen and 340% excess oxygen in the stream.

0378-7753/$ – see front matter
doi:10.1016/j.jpowsour.2005.05.074

Table 1
Inlet conditions and parameters

Anode channel inlet conditions	
Velocity ($m\,s^{-1}$)	1.2
Mole fraction of H_2	0.759
Mole fraction of H_2O	0.241
Dew-point temperature (°C)	65
Cathode channel inlet conditions	
Velocity ($m\,s^{-1}$)	4.5
Mole fraction of O_2	0.170
Mole fraction of N_2	0.638
Mole fraction of H_2O	0.192
Dew-point temperature (°C)	57
Operating conditions	
Operating pressure (kPa)	101
Permeability of diffusion layer (m^2)	3.3×10^{-15}
Membrane thickness (μm)	50
Density of dry membrane ($kg\,m^{-3}$)	2000
Equivalent weight of a dry membrane ($kg\,mol^{-1}$)	1.1
Oxygen exchange current density ($A\,m^{-2}$)	140
Hydrogen exchange current density ($A\,m^{-2}$)	1000

a constant flow rate of $90\,cm^3\,s^{-1}$ and $355\,cm^3\,s^{-1}$ for the anode/cathode respectively at 101 kPa and 70 °C for $0.33\,A\,cm^{-2}$ at 0.7 V). The simulation used a commercial computational fluid dynamics (CFD) solver, Star-CD Version 3.2, with modified subroutines to account for the electrochemical reactions of hydrogen and oxygen and the transport of water through the membrane and catalysts layer. The complete 3D Navier–Stokes equations were solved with a control-volume-based discretization of the computational domain and the velocity and pressure distribution in the flow channels and the gas diffusion layer were obtained for every time-step.

In contract to part I, we present here predictions to discuss the behavior when the fixed flow rates correspond to normal and maximum utilization (i.e., changes in stoichiometry from 1.45/2.42 to 1.05/1.73). That is, in an effort to expand the understanding the behavior of a PEMFC, we present here a study that focuses on changes in the cell voltage between 0.7 V and 0.5 V for a stoichiometry of 1.45/2.42 for the 0.7 V conditions (i.e., $0.33\,A\,cm^{-2}$). The operation at 0.5 V results in almost complete utilization of the hydrogen and perhaps a mass transfer limitation of the oxygen. We call this 1.05/1.73 stoichiometry a "minimal" stoichiometric condition because the cell operated a fixed voltage cannot exhibit truly starved condition (i.e., the current will adjust to the supply of fuel).

This numerical simulation uses the same transient, isothermal, 3D mass transfer model and serpentine gas-flow-channel geometry as part I. The operating conditions and model parameters of this work are shown in Table 1. The transient load profile consists of changing the cell voltage from 0.7 V at steady state to 0.5 V and from 0.5 V at steady state to 0.7 V at an average rate of $1\,V\,s^{-1}$. This rate was not linear as shown in Table 2 because we followed the output from an experimental load. As discussed in part I, the predictions were grid and time-step independent.

2. Results and discussion

Fig. 1 shows how the averaged current density changes when the cell voltages are changed from 0.5 V to 0.7 V and from 0.7 V to 0.5 V. The average is obtained by multiplying the current in each grid cell by the surface area of each cell, summing the resulting current, and then dividing this current by $10\,cm^2$. Fig. 1a shows undershoot in the current density when the cell voltage is increased. The lowest averaged current density is $0.23\,A\,cm^{-2}$ when the cell voltage reaches 0.685 V, and then it increases and reaches a steady-state value at $0.33\,A\,cm^{-2}$. Note that the flow condition at 0.7 V corresponds to stoichiometries of 1.45/2.42 at $0.33\,A\,cm^{-2}$ and that at 0.5 V these conditions correspond to stoichiometries of 1.05/1.73 for $0.46\,A\,cm^{-2}$. This decrease of about $0.22\,A\,cm^{-2}$ is comparable with the data of Ref. [1] even though the average rate of voltage change was $0.22\,V\,s^{-1}$ instead of the $1.0\,V\,s^{-1}$ used here. The time constants are similar due to the differences in the rate of voltage change. Fig. 1b shows overshoot behavior. The averaged current density increases from $0.33\,A\,cm^{-2}$ to $0.96\,A\,cm^{-2}$ when the cell voltage is 0.52 V and then the current density decreases and reaches the steady state at $0.46\,A\,cm^{-2}$. This is the same current density as that shown at 0.5 V in Fig. 1a. Note that

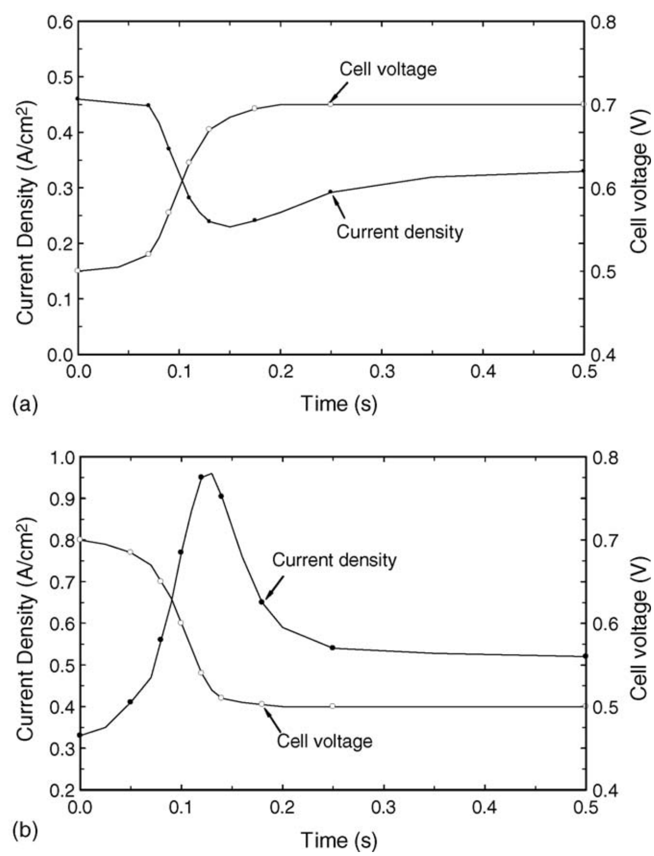

Fig. 1. (a) Averaged current density for change from 0.5 V to 0.7 V. Open circles indicate cell voltage and filled circles indicate current density and (b) averaged current density for change from 0.7 V to 0.5 V and open circles indicate cell voltage and filled circles indicate current density.

Table 2
Cell voltage changes from 0.5 V to 0.7 V in 0.2 s and from 0.7 V to 0.5 V in 0.2 s

Time (s)	0.0	0.02	0.04	0.07	0.08	0.09	0.10	0.11	0.12	0.13	0.15	0.175	0.2
Cell voltage (V)	0.50	0.5025	0.505	0.52	0.54	0.57	0.60	0.63	0.65	0.67	0.685	0.695	0.70
Time (s)	0.0	0.025	0.05	0.07	0.08	0.09	0.10	0.11	0.13	0.14	0.16	0.18	0.2
Cell voltage (V)	0.70	0.695	0.685	0.67	0.65	0.63	0.60	0.57	0.52	0.51	0.505	0.5025	0.50

the symbols shown in Fig. 1 and subsequent figures are for convenience and that they are not related to the true stepping of the numerical integration. The height of the overshoot and undershoot can be changed by the rate of cell voltage change and by the flow rates (see the discussion by Shimpalee et al. [4] for the case of excess stoichiometry), but those changes are not the focus of our work here. Instead, here we fix the rate of voltage change and flow rate and study the dependent variables in order to understand their interactions during current overshoot/undershoot behavior. It may be interesting to note that the overshoot in Ref. [1] is only 0.4 A cm^{-2} for an average voltage rate of 0.22 V s^{-1}.

Fig. 2 shows the variation of the averaged values of variables to be studied in this paper. These variables are net water flux per proton (Alpha), oxygen mole fraction, and hydrogen mole fraction. As discussed above, the equations for these variables are shown in Tables 1 and 2 of Ref. [2]. Consider the change from a "minimal O_2" condition to a "typical O_2" concentration when the cell voltage is increased from 0.5 V to 0.7 V as shown in Fig. 2a. Here, the averaged net water flux per proton decreases until the cell voltage reaches 0.57 V and then it shows its own overshoot behavior before it reaches a steady-state value after the cell voltage reaches 0.7 V. During this change, the oxygen mole fraction and the hydrogen mole fraction increase and also reach steady-state values substantially after the voltage has reached 0.7 V (i.e., at 0.5 s for the mole fractions versus 0.2 s for the voltage). As discussed in part I, Alpha is the sum of the electro-osmotic drag of water and the diffusion of water from the cathode to the anode. It is negative when the water back diffusion is greater than the electro-osmotic drag and this occurs when the membrane is thin and the cathode water activity at the membrane surface is larger than the anode water activity. The negative average value at 0.5 V also results from the operating conditions and the minimal flow rates. Fig. 2b shows the relationship of these variables when the cell voltage is changed from 0.7 V to 0.5 V in 0.2 s. When the cell voltage is decreased, the mole fractions of oxygen and hydrogen are lowered due to the increased current. At voltage of 0.505 V, water back diffuses to the anode through the MEA as indicated by the negative value of Alpha. The change of Alpha lags the change in voltage.

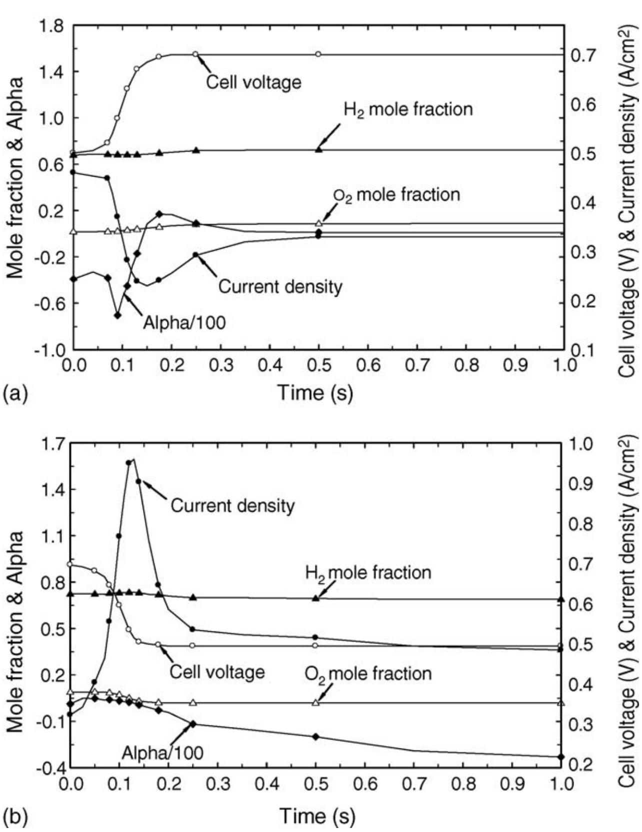

Fig. 2. (a) Averaged cell variables during undershoot behavior and (b) averaged cell variables during overshoot behavior.

It may be important to note that these predictions do not accurately account for water phase change caused by a distribution in the temperature and activity of water in each stream. In fact some of the predicted local activities exceed 1.0 during the simulation and thus the possibility of condensation was indicated. In defense of the predictions and the discussion here, it is our experience with steady-state calculations that the local temperature increases at high reaction rates so that the local water activities decrease when the energy balance is included. Thus, the predictions here will show slightly higher currents and lower mole fractions because local activities greater than 1.0 increase local conductivity and because condensation will block some reaction sites. Again, we show and discuss these transient isothermal predictions because they provide a less computationally intensive solution to the transient problem and because it is our experience that the isothermal equations provide the same general trends as a more complete equation set.

To further explain the overshoot and undershoot behaviors, let us examine the local profiles at the MEA surface at $x = 0.016$ m across the serpentine flow path as shown in Fig. 3. Fig. 4a and b illustrates the changes in the local current density profiles at different cell voltages and times. Fig. 4a shows the transient local current density profiles when the cell voltage is changed from 0.5 V to 0.7 V and Fig. 4b presents the profiles when the cell voltage is changed from 0.7 V to 0.5 V. In Fig. 4a, when the cell voltage is 0.5 V and a steady state

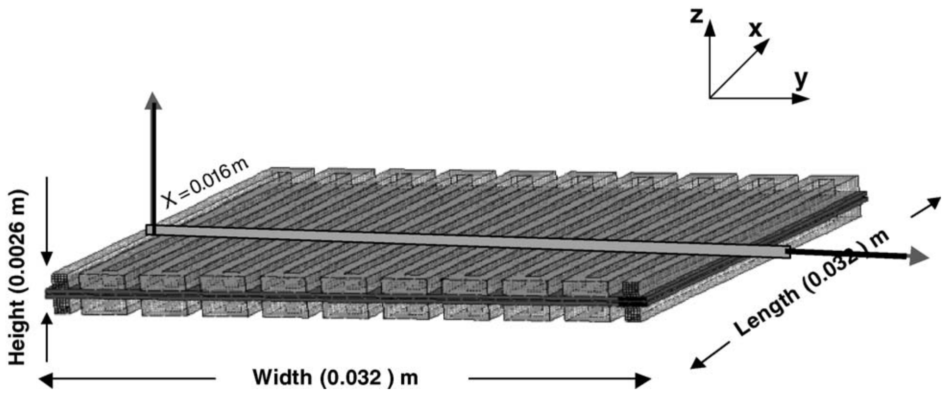

Fig. 3. The grid geometry of 10 cm^2 PEMFC with the location where the local profiles at the MEA surface across the serpentine flow path and electrode width are presented.

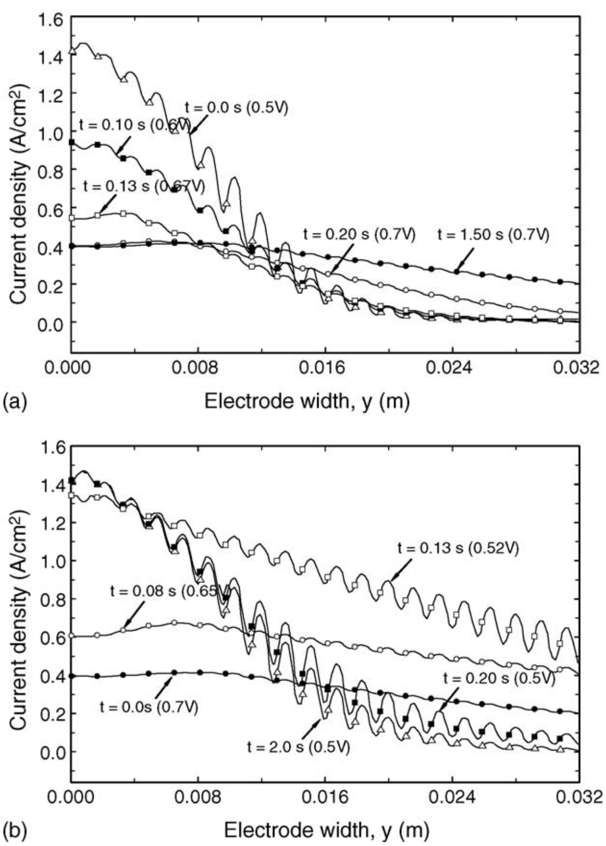

Fig. 4. (a) Variation of current density along electrode width at $x = 0.016$ m at different times for undershoot behavior and (b) variation of current density along electrode width at $x = 0.016$ m at different times for overshoot behavior.

is maintained, the local current density profile is highly non-uniform. The largest current density is at the inlet region ($y = 0.0$ m) with the value of 1.46 A cm^{-2} and the lowest is at the outlet region ($y = 0.032$ m) with the value of almost 0.0 A cm^{-2}. Further, there is the appearance of oscillatory behavior in local current density profile due to the rib spacing between the flow channels. These areas are most restricted to mass transfer and they respond to load changes at rates different from the area adjacent to the flow channels. According to Fig. 4a, as the cell voltage is increasing, the local current density profile is becoming uniform with decreasing local values in the first half of the cell (from inlet to about the center) and increasing of the local current density values in the second half of the cell (from center to outlet). At a time of 0.13 s (i.e., at cell voltage of 0.67 V), the current density profile is at about the valley of the current undershoot. On the other hand, when the cell voltage is decreased from 0.7 V to 0.5 V, Fig. 4b shows that the local current density profile increases in a somewhat uniform distribution until it reaches the highest profile at a cell voltage of 0.52 V (i.e., 0.13 s). After that, the current density profile becomes more non-uniform with the significant decreases in local current density from the center of the cell toward the outlet region. The local current density changes from a linear profile with width until about 0.13 s (0.52 V) and then the starved conditions produce an exponential distribution after 0.2 s. The reasons for the overshoot/undershoot behavior of current can be discussed by considering the distributions of oxygen concentration and Alpha as shown in Figs. 5 and 6.

Fig. 5a and b shows the transient distributions of local oxygen mole fraction across the electrode width for the undershoot (cell voltage changes from 0.5 V to 0.7 V) and overshoot conditions (cell voltage change from 0.7 V to 0.5 V). As shown in Fig. 5a at a cell voltage of 0.5 V and steady state, the distribution of oxygen mole fraction is similar to the current density profile due to fixed flow rates corresponding to a starved condition. That is, the oxygen mole fraction decreases along the electrode width from inlet toward the outlet especially in the first half of the cell where the reaction rate is high. Oxygen is almost depleted in the second half of the cell (i.e., a mole fraction between 0.01 and 0.005) and this limits the current density in these locations. Then, when the cell voltage is increased, the rate of gas consumption is decreased and the oxygen mole fractions increase. Note that the non-uniform profile indicates a time lag of at least 0.13 s (i.e., a cell voltage of 0.67 V) before there is significant reaction toward the outlet and that this lag agrees with the current

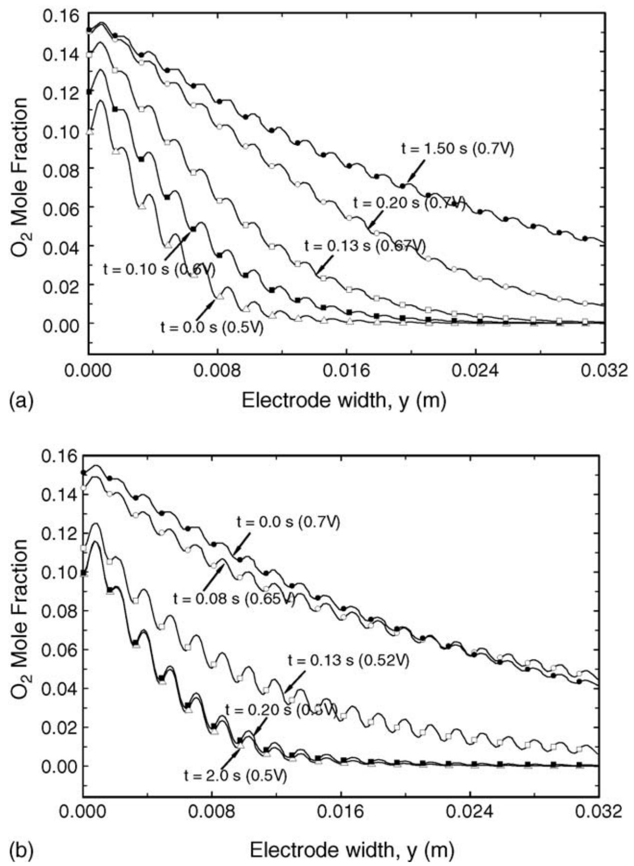

Fig. 5. (a) Variation of oxygen mole fraction along electrode width at $x = 0.016$ m at different times for undershoot behavior and (b) variation of oxygen mole fraction along electrode width at $x = 0.016$ m at different times for overshoot behavior.

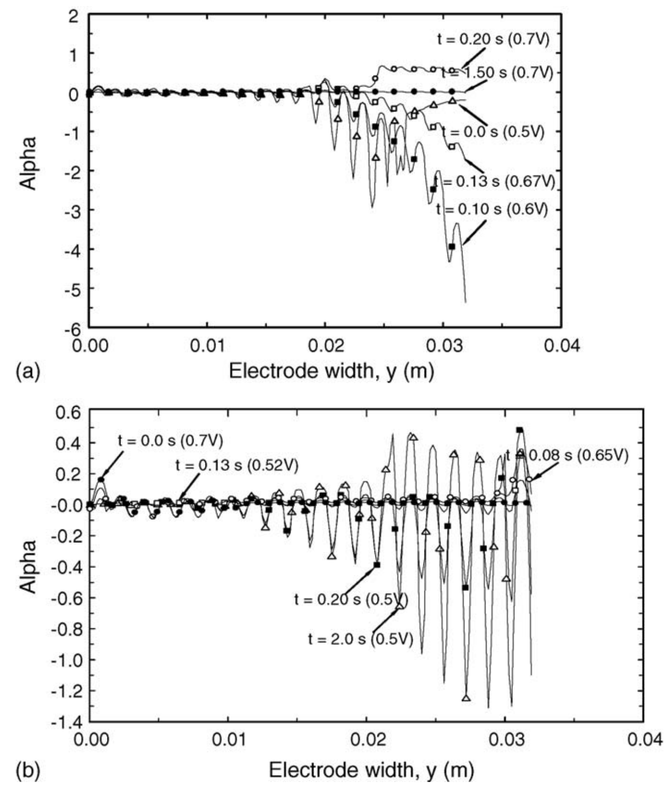

Fig. 6. (a) Variation of net water flux (Alpha) along electrode width at $x = 0.016$ m at different times for undershoot behavior and (b) variation of net water flux (Alpha) along electrode width at $x = 0.016$ m at different times for overshoot behavior.

undershoot presented in Fig. 1a. This is because there is a residence time delay of $0.15\,s$[2] where the unreacted gases have not passed from the inlet to the gas depleted locations. After 0.2 s, the local oxygen distributions become more uniform with significantly increased values in second half of the cell. This corresponds with the increasing local current density as shown in Fig. 4a for $y > 0.016$ m at $t = 0.2$ s.

When the cell voltage is decreased from 0.7 V to 0.5 V, the reaction rate is increased and the rates of gases consumption increase along with the rate of cathode water production. Fig. 5b shows the distributions of oxygen mole fraction that can be compared with Fig. 5a. The non-uniformity of oxygen distribution increases as the reaction rate increases. Consequently, the depletion of the reacting gases, especially oxygen, does not occur until after the current density reaches the peak of overshoot (cell voltage = 0.52 V and time = 0.13 s). This depletion creates the reduction in current density shown in Fig. 4b.

Fig. 6 shows the transient distributions of local net water flux per proton across the electrode width during the observed undershoot and overshoot behavior. Fig. 6a shows the transient water flux distributions when the cell voltage is increased from 0.5 V to 0.7 V. At steady state with 0.5 V and at time equals 0.1 s with 0.6 V, the large negative values, indicating significant back diffusion, are most noticeable. Thus, even though the current density is low, any water produced or carried downstream from the first half of the cell, diffuses to anode. The large differences between the area under the ribs and the area in the channel show the effect of oxygen mass transfer resistance. When the cell voltage is increased with time, the difference between electro-osmotic transport and back diffusion is reduced due to the supply of oxygen to the cathode, the supply of hydrogen to the anode, and the resumption of current in the second half of the cell. Similar profiles are shown in Fig. 6b when the cell voltage is decreased from 0.7 V to 0.5 V.

The undershoot/overshoot behavior of the PEMFC performance can now be summarized based on the discussion of Figs. 2–6. For undershoot behavior, the reaction rate is reduced due to increasing the cell voltage faster than the oxygen that can replenish the starved locations. That is, the decrease in current density and the lowest value of the current density is reached when the partial pressure of oxygen at the downstream (starved) location starts to increase. Thus, as the oxygen is replenishing the depleted zones, the cell current (and geometric averaged current density) increases.

[2] Calculated with $v = 4.5\,m\,s^{-1}$ at the cathode side and a channel length of 0.66 m for the single pass cell. Note that consumption of the gas reduces the velocity along the channel length and that this gives a longer delay.

These figures confirm that the rate of increase in oxygen mole fraction is slower than the increase in cell voltage. For the overshoot behavior, the reaction rate is increased because of the lowering of the cell voltage. Thus, the current density increases and reaches the maximum averaged value before the oxygen starts to diminish in the second half of the cell. This lower oxygen in the second half of the cell leads to the oxygen starved operating condition. Thus, the rapid lowering of the local current density value correlates with the time at which the oxygen starts to decrease.

3. Conclusions

A 3D transient simulation of PEM fuel cell was studied at minimal stoichiometric fixed flow rates of feed gases. The flow rates correspond to normal fuel and oxygen utilization at the high cell voltage and a minimal operating condition at the low cell voltage. The cell voltage was changed at a somewhat rapid rate of $1.0\,\mathrm{V\,s^{-1}}$ and modest undershoot and overshoot behavior in the current was observed and explained in terms of the distributions of current density, oxygen concentration, and net water transport.

For a change from a minimal condition, the results indicate that when the cell voltage is increased, the response in the local current density decreases faster than the flow of oxygen can replenish the regions that experience a starvation of O_2. Then, the current density increases after oxygen is relished and the current distribution becomes more uniform. When the cell voltage is decreased, the current density increases and reaches the peak of overshoot while the capacity of the oxygen in the flow channels is used. Then, as the local partial pressure decreases toward the exit of the cell, the geometric averaged current density starts to decrease toward the steady-state value. This steady-state value corresponds to a highly non-uniform local current density distribution, dependent on local concentrations of the reacting gases. For these conditions, oxygen appears to control the distribution. These results may help effort in the design of the flow-field and manifold configuration. These design changes may improve stack performance.

Acknowledgements

The authors wish to acknowledge the financial support of this work by the South Carolina State University/University Transportation Center (Grant #2000-013), the Department of Energy-EPSCoR (Cooperative Agreement Grant #DE-FG02-91ER75666), and the Office of Naval research (Grant #N00014-98-1-0554).

References

[1] S.-H. Kim, S. Shimpalee, J.W. Van Zee, J. Electrochem. Soc. 152 (2005) A1265–A1271.
[2] S.-H. Kim, S. Shimpalee, J.W. Van Zee, J. Power Sources 137 (2004) 43–52.
[3] S.-H. Kim, S. Shimpalee, J.W. Van Zee, J. Power Sources 135 (2004) 110–121.
[4] S. Shimpalee, W.-K. Lee, J.W. Van Zee, H. Naseri-Neshat, J. Power Sources 156 (2006) 355.